18. R. Roth, H. Feldmaier, *Phys. Rev. A* **65**, 021603(R) (2001).
19. For $N_{Rb} = 10^5$ and $N_K = 3 \times 10^4$, the expected dimensions of the pure BEC are $R_R = 2.8$ μm and $R_A = 37$ μm, whereas the Fermi gas is 2.2 times larger, in accordance with the experimental observation. Although the centers of mass of K and Rb are slightly displaced by gravity, their overlap is not substantially affected.
20. We measured a_{BF} by studying the damping of relative oscillations of the two species in the magnetic trap. This value is somewhat larger than the one previously measured with a different technique (*8*), though consistent also with our original prediction (*15*).
21. For $N_{Rb} = 10^5$ and $N_K = 3 \times 10^4$, the peak densities for the two noninteracting gases are $n_{Rb} = 2 \times 10^{14}$ cm^{-3} and $n_K = 8 \times 10^{12}$ cm^{-3}.
22. R. Roth, *Phys. Rev. A* **66**, 013614 (2002).
23. Given our detection limits, this corresponds to $T < 0.67T_C = 0.3T_F$.
24. L. Viverit, *Phys. Rev. A* **66**, 023605 (2002).
25. ———, S. Giorgini preprint available at http://arXiv.org/abs/cond-mat/0207260.
26. M. Holland, S. J. J. M. F. Kokkelmans, M. L. Chiofalo, R. Walser, *Phys. Rev. Lett.* **87**, 120406 (2001).
27. W. Hofstetter, J. I. Cirac, P. Zoller, E. Demler, M. D. Lukin, preprint available at http://arXiv.org/abs/cond-mat/0204237.

28. We acknowledge stimulating discussions with R. Roth, G. Shlyapnikov, and L. Viverit. Supported by Ministero dell'Instruzione, dell'Universitá e Ricerca, by the European Community under contract HPRICT1999-00111, and by INFM, Progetto di Ricerca Avanzata "Photonmatter." G.R. is also at Dipartimento di Fisica, Università di Trento; F.F. and M.I. are also at Dipartimento di Fisica, Università di Firenze; and R.B. is also at Department of Physics, University of Dayton, OH.

15 August 2002; accepted 20 August 2002
Published online 29 August 2002;
10.1126/science.1077386
Include this information when citing this paper.

Efficient Photochemical Water Splitting by a Chemically Modified n-TiO_2

Shahed U. M. Khan,* Mofareh Al-Shahry, William B. Ingler Jr.

Although n-type titanium dioxide (TiO_2) is a promising substrate for photogeneration of hydrogen from water, most attempts at doping this material so that it absorbs light in the visible region of the solar spectrum have met with limited success. We synthesized a chemically modified n-type TiO_2 by controlled combustion of Ti metal in a natural gas flame. This material, in which carbon substitutes for some of the lattice oxygen atoms, absorbs light at wavelengths below 535 nanometers and has a lower band-gap energy than rutile (2.32 versus 3.00 electron volts). At an applied potential of 0.3 volt, chemically modified n-type TiO_2 performs water splitting with a total conversion efficiency of 11% and a maximum photoconversion efficiency of 8.35% when illuminated at 40 milliwatts per square centimeter. The latter value compares favorably with a maximum photoconversion efficiency of 1% for n-type TiO_2 biased at 0.6 volt.

Since the discovery (*1*) of photoelectrochemical splitting of water on n-TiO_2 electrodes, semiconductor-based photoelectrolysis of water to hydrogen and oxygen has received much attention (*2–7*). Some applications include the use of n-TiO_2 in wet solar cells (*8–10*) and for the photodegradation of organics present in polluted water and air (*11, 12*) under ultraviolet (UV) light (wavelength $\lambda < 400$ nm) illumination, the energy of which exceeds the band-gap energy of 3.0 eV in the rutile crystalline form of n-TiO_2. Efficient photosplitting of water to hydrogen, a source of abundant clean energy, requires photoelectrodes that (i) are highly stable, (ii) are inexpensive, (iii) have a conduction band minimum that is higher than the H_2/H_2O level and a valence band maximum that is lower than the H_2O/O_2 level, and (iv) can absorb most of the photons of the solar spectrum. Although both the anatase and rutile forms of n-TiO_2 meet the first three of these conditions, they are poor absorbers of photons in the solar spectrum. Several attempts have been made to lower the band-gap energy of n-TiO_2 by transition metal doping (*13–16*) and reduction by hydrogen (*17, 18*), but no noticeable change in band-gap energy of n-TiO_2 was observed. Recently, Asahi *et al.* (*19*) reported that nitrogen doping of n-TiO_2 to n-$TiO_{2-x}N_x$ shifted its optical absorption and photodegradation of methylene blue and gaseous acetaldehyde in the visible region of $\lambda < 500$ nm.

We therefore synthesized a chemically modified (CM) n-TiO_2 by flame pyrolysis of Ti metal sheet in an attempt to lower its band-gap energy so that it could absorb the UV and most of the visible light of the solar spectrum while retaining its stability. We thermally pyrolyzed a Ti metal sheet 0.25 mm thick (Strem Co.) in the presence of combustion products [CO_2 and steam (H_2O)] in a natural gas flame with controlled amounts of oxygen added at a flow rate of ~350 ml min^{-1}. The flame temperature, measured with a digital pyrometer (Thermolyne Co.), was maintained close to 850°C by controlling the flow rates of natural gas and oxygen. The best photoresponse was obtained with a pyrolysis time of 13 min. The CM-n-TiO_2 films were dark gray, whereas the n-TiO_2 films prepared in an electric tube furnace under the same oxygen flow rate, at the same temperature and time of pyrolysis (considered here as a reference sample of n-TiO_2 film), were very light gray.

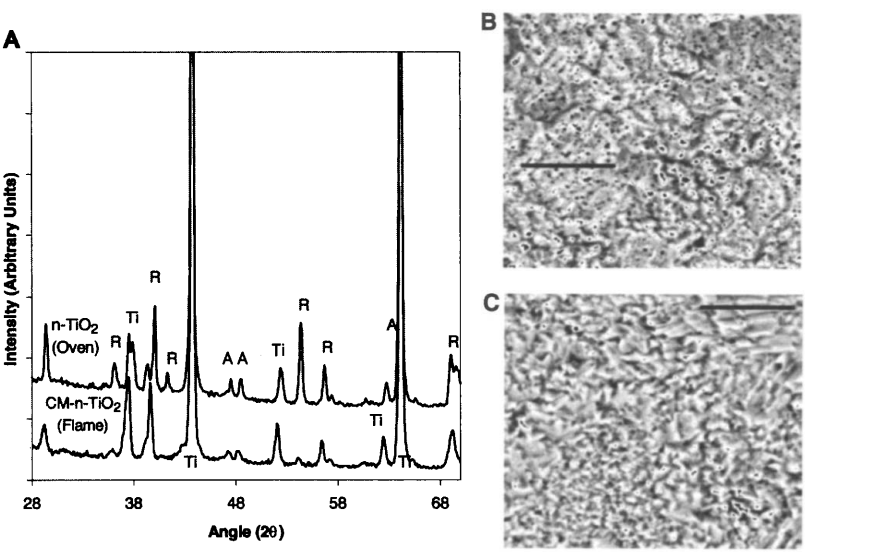

Fig. 1. (**A**) X-ray diffraction (XRD) pattern for a CM-n-TiO_2 (flame-made) and the reference n-TiO_2 (electric tube furnace– or oven-made) photoelectrodes. Ti, titanium metal; A, anatase peaks; R, rutile peaks. (**B** and **C**) SEM images of CM-n-TiO_2 (flame-made) sample (B) and reference n-TiO_2 (electric tube furnace– or oven-made) sample (C). Scale bars, 20 μm.

Department of Chemistry and Biochemistry, Duquesne University, Pittsburgh, PA 15282, USA.

*To whom correspondence should be addressed. E-mail: khan@duq.edu

The x-ray diffraction (XRD) of the CM-n-TiO_2 film showed mainly rutile structure (Fig. 1A). However, the reference n-TiO_2 film shows a mixture of rutile and anatase crystalline forms (Fig. 1A). The scanning electron microscopic (SEM) results indicate that CM-n-TiO_2 is more porous (represented by more dark spots) compared to a reference n-TiO_2 sample (Fig. 1, B and C). X-ray photoelectron spectroscopic (XPS) data indicate an average composition of CM-n-TiO_2 to be n-$TiO_{2-x}C_x$, where x is ~0.15. The presence of CO_2, a combustion product in the natural gas flame at 850°C, facilitated the incorporation of carbon in the n-TiO_2 films. The presence of steam (H_2O) in the flame is expected to enhance the rate of titanium oxide film formation (*20*). The XPS analysis also showed the absence of N and H in both CM-n-TiO_2 and the reference n-TiO_2 films. The optical absorption spectra (Fig. 2) show that CM-n-TiO_2 films absorb appreciably at wavelengths less than 535 nm (which corresponds to a band-gap energy of 2.32 eV), whereas reference n-TiO_2 samples do not. The CM-n-TiO_2 films show two optical absorption thresholds at 535 and 440 nm (Fig. 2) in the visible range, whereas the reference n-TiO_2 shows only one at 414 nm, which corresponds to a band-gap energy of 3.0 eV (Fig. 2). These two absorption thresholds indicate two possible compositions of chemically modified n-$TiO_{2-x}C_x$.

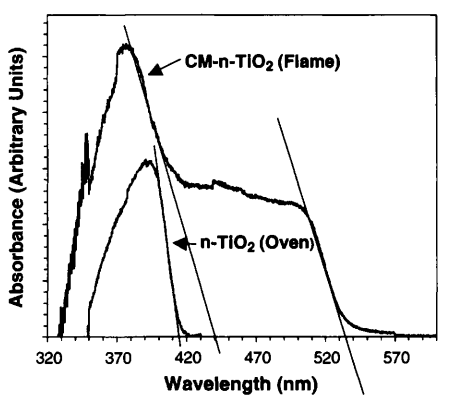

Fig. 2. The UV-visible spectra of CM-n-TiO_2 (flame-made) and reference n-TiO_2 (electric tube furnace– or oven-made). The flame-made sample shows threshold wavelengths of 535 nm (band gap of 2.32 eV) and 440 nm (band gap of 2.82 eV); the electric tube furnace– or oven-made sample shows a threshold wavelength of 414 nm (band gap of 3.0 eV).

The photoresponse of CM-n-TiO_2 films was evaluated by measuring the rate of water-splitting reaction to hydrogen and oxygen, which is proportional to photocurrent density j_p. We verified that H_2 and O_2 are the photoproducts by gas chromatographic (GC) analysis using a SRI 8610 chromatograph equipped with a thermal conductivity detector (TCD). Also, GC analysis using a Perkin Elmer 8500 chromatograph equipped with TCD showed the absence of CO and CO_2 in the photoproducts. Furthermore, we collected gaseous photoproducts and observed an exact 2:1 volume ratio of H_2 and O_2, which further confirmed water-splitting.

Photocurrents were measured with a CM-n-TiO_2 sample (area 0.2 cm^2) under illumination from a 150-W xenon arc lamp (Hanovia) fitted with an infrared light filter (*21*). Photocurrent densities j_p (which correspond to rates of production of hydrogen and oxygen) from the water-splitting reaction at CM-n-TiO_2 under illumination of light of power density 40 mW cm^{-2} from a 150-W xenon lamp are shown in Fig. 3 as a function of applied potential E_{app}. The observed dark current densities were found to be negligible (Fig. 3).

The maximum photoconversion efficiency ε_{eff} (photo) of 8.35% (which corresponds to a total conversion efficiency of 11.0%) was observed at a minimal applied potential of 0.30 V with a photocurrent density of 3.60 mA cm^{-2} (Fig. 4) when ε_{eff} (photo) was calculated using an efficiency equation [Eq. 1 (*22*)] in which the contribution due to applied potential was subtracted from the total efficiency. However, under similar conditions of illumination, a maximum ε_{eff} (photo) of 1.08% was observed at a higher applied potential of 0.60 V for the reference n-TiO_2 samples under 150-W xenon lamp illumination (Fig. 4). These results confirm that flame pyrolysis chemically modified n-TiO_2 and lowered its band-gap energy to a minimum value of 2.32 eV to absorb visible light. Photoconversion efficiency did not decrease during successive tests with illumination intensity of 40 mW cm^{-2} over a period of 6 months. Hence, the lowering of the band-gap energy did not affect the stability of CM-n-TiO_2.

References and Notes

1. A. Fujishima, K. Honda, *Nature* **238**, 37 (1972).
2. J. R. Bolton, *Sol. Energy* **57**, 37 (1996).
3. S. U. M. Khan, J. Akikusa, *J. Phys. Chem. B* **103**, 7184 (1999).
4. J. Akikusa, S. U. M. Khan, *J. Electrochem. Soc.* **145**, 89 (1998).
5. S. U. M. Khan, J. Akikusa, *Int. J. Hydrogen Energy* **27**, 863 (2002).
6. O. Khaselev, J. A. Turner, *Science* **280**, 425 (1998).
7. S. Licht *et al.*, *J. Phys. Chem.* **104**, 8920 (2000).
8. B. O'Regan, M. Gratzel, *Nature* **353**, 737 (1991).
9. G. R. Comte, M. Gratzel, *Sol. Energy Mater. Sol. Cells* **58**, 321 (1999).
10. G. Sauve *et al.*, *J. Phys. Chem. B* **104**, 3488(2000).
11. M. R. Hoffman *et al.*, *Chem. Rev.* **95**, 69 (1995).
12. D. S. Ollis, H. Al-Ekabi, Eds., *Photocatalytic Purification and Treatment of Water and Air* (Elsevier, Amsterdam, 1993).
13. A. K. Ghosh, G. P. Maruska, *J. Electrochem. Soc.* **24**, 1516 (1977).
14. W. Choi, A. Termin, M. R. Hoffmann, *J. Phys. Chem.* **98**, 13669 (1994).
15. M. Anpo, *Catal. Surv. Jpn.* **1**, 169 (1997).
16. J. Akikusa, thesis, Duquesne University (1997).
17. R. G. Breckenridge, W. R. Hosler, *Phys. Rev.* **91**, 793 (1953).
18. D. C. Cronemeyer, *Phys. Rev.* **113**, 1222 (1959).
19. R. Asahi, T. Morikawa, T. Ohwaki, K. Aoki, Y. Taga, *Science* **293**, 269 (2001).
20. Y. Wouters, A. Galerie, J. P. Petit, *Solid State Ionics* **104**, 89 (1997).

21. This xenon arc lamp can generate maximum half of the power density (50 mW cm^{-2}) of air mass 1.5 (*23*). The electrical contact was made with Ti metal substrate by using silver epoxy connected to a copper wire. A conventional three-electrode configuration in a single-compartment cell was used with CM-n-TiO_2 film, platinum foil, and a saturated

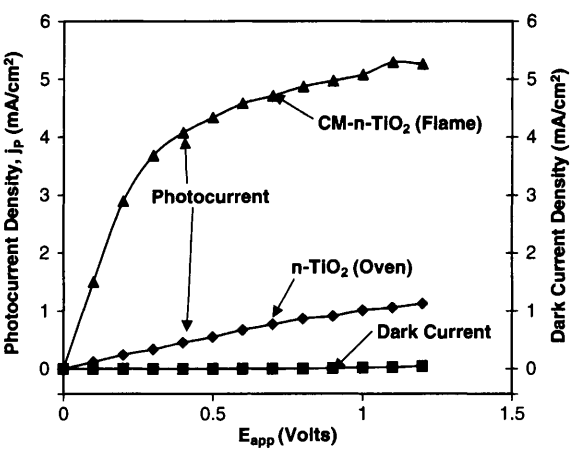

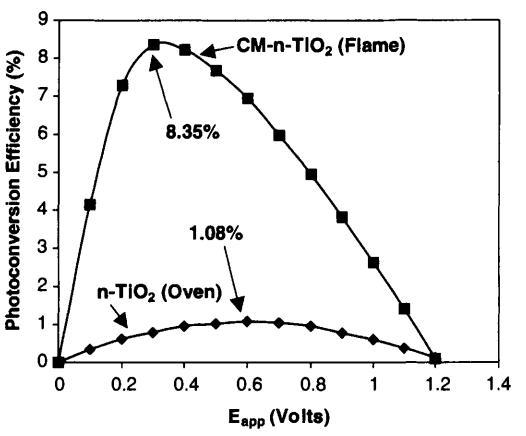

Fig. 3 (left). Photocurrent density j_p as a function of applied potential E_{app} at CM-n-TiO_2 (flame-made) and the reference n-TiO_2 (electric tube furnace– or oven-made) photoelectrodes under xenon lamp illumination at an intensity of 40 mW cm^{-2}. Dark current densities at CM-n-TiO_2 (flame-made) as a function of applied potential are also shown. **Fig. 4 (right).** Photoconversion efficiency as a function of applied potential E_{app} at CM-n-TiO_2 (flame-made) and the reference n-TiO_2 (electric tube furnace– or oven-made) photoelectrodes under xenon lamp illumination at an intensity of 40 mW cm^{-2}.

calomel electrode (SCE) as the working, counter, and reference electrodes, respectively. Photocurrents as a function of electrode potential were measured with an EG & G 362 scanning potentiostat and recorded with an X-Y recorder (Houston Instruments, model RE0092). The intensity of the light source (in mW cm^{-2}) was measured by a radiometer (International Light Co., model IL 1350). The electrolyte, 5 M KOH, was freshly prepared using double-deionized water with resistivity of 18 megohms cm^{-1}. All solutions were prepared from analytical-grade reagents.

22. The photoconversion efficiency ε_{eff} (photo) of light energy to chemical energy in the presence of an external applied potential E_{app} can be expressed as

$$\% \ \varepsilon_{eff}(\text{photo}) = [j_p(E^0_{rev} - |E_{app}|) \times 100/(I_0)] \quad (1)$$

(3–5), where j_p is the photocurrent density, E^0_{rev} is the standard state-reversible potential (which is 1.23 V for the water-splitting reaction), I_0 is the intensity (power density) of the incident light, and $|E_{app}|$ is the absolute value of the applied potential E_{app}, which is obtained as

$$E_{app} = (E_{meas} - E_{aoc}) \quad (2)$$

(3–5), where E_{meas} is the electrode potential at which j_p was measured, and E_{aoc} is the electrode potential at open circuit in the same electrolyte solution and under the same illumination of light at which j_p was measured. For the CM-n-TiO_2 electrode, E_{aoc} = −1.0 volt/SCE was observed at illumination intensity of 40 mW cm^{-2} in 5 M KOH solution; E_{meas} and E_{doc} were with respect to the same reference electrode (SCE). Note that the total conversion efficiency of light and electrical energy to chemical energy, ε_{eff} (total), was calculated by neglecting E_{app} in Eq. 1.

23. R. E. Bird, R. L. Hulstrom, L. J. Leis, *Sol. Energy* **30**, 563 (1983).

13 June 2002; accepted 29 August 2002

The Origin of Aluminum Flocs in Polluted Streams

Gerhard Furrer,[1]* Brian L. Phillips,[2] Kai-Uwe Ulrich,[3] Rosemarie Pöthig,[4] William H. Casey[5]*

About 240,000 square kilometers of Earth's surface is disrupted by mining, which creates watersheds that are polluted by acidity, aluminum, and heavy metals. Mixing of acidic effluent from old mines and acidic soils into waters with a higher pH causes precipitation of amorphous aluminum oxyhydroxide flocs that move in streams as suspended solids and transport adsorbed contaminants. On the basis of samples from nine streams, we show that these flocs probably form from aggregation of the ε-Keggin polyoxocation $AlO_4Al_{12}(OH)_{24}(H_2O)_{12}^{7+}$(aq) ($Al_{13}$), because all of the flocs contain distinct $Al(O)_4$ centers similar to that of the Al_{13} nanocluster.

In studies of the aluminum geochemistry of acid mine drainage (*1*, *2*), solids were identified that precipitate at 4.2 < pH < 4.9 as either x-ray–amorphous $Al(OH)_3$ or microcrystalline gibbsite. These flocs are fluffy (Fig. 1) and form as acidic effluent enriched in dissolved aluminum mixes with near-neutral surface water. A similar phenomenon occurs in watersheds where the load of acid rain critically exceeds the buffering capacity of the soil and parent rock (*3*). It is thought (*4*) that the flocs form by aggregation of monomeric aluminum complexes into a $Al_6(OH)_{12}(H_2O)_{12}^{6+}$ multimer that is structurally similar to dioctahedral sheets of gibbsite. Dissolved $Al_6(OH)_{12}(H_2O)_{12}^{6+}$, however, has never been detected, and this model has been challenged (*5*).

Here we propose an alternative explanation. We examined flocs from nine polluted streams in Germany and California (Table 1) (table S1 and figs. S2 to S4) with ^{27}Al magic-angle spinning (MAS) nuclear magnetic resonance (NMR) spectroscopy, which resolves aluminum atoms with different coordination environments. The ^{27}Al NMR spectra of all field samples exhibit signals near +63 and +35 parts per million (ppm), which indicate the presence of substantial amounts of aluminum in tetrahedral form [$Al(O)_4$] and in coordination to five oxygen atoms [$Al(O)_5$] (*6*), in addition to the dominating $Al(O)_6$ peak near +7 ppm. Because the spectra of all samples were similar, we selected three samples to show the range in relative intensities (Fig. 2A). The first and last samples (Fig. 2A, top and bottom) have the most and least amounts of $Al(O)_4$, respectively. The sec-

Fig. 1. Aluminum oxyhydroxide floc on a streambed in Yuba County, California. The white aluminum oxyhydroxide floc overlies orange iron oxyhydroxide solids. Image width, ≈30 cm.

[1]Institute of Terrestrial Ecology, Eidgenössische Technische Hochschule Zürich, Grabenstrasse 3, CH-8952 Schlieren, Switzerland. [2]Department of Geosciences, State University of New York, Stony Brook, NY 11794–2100, USA. [3]Technical University of Dresden, Ecological Station Neunzehnhain, D-09514 Lengefeld, Germany. [4]Leibniz Institute of Freshwater Ecology and Inland Fisheries, Müggelseedamm 310, D-12587 Berlin, Germany. [5]Department of Land, Air, and Water Resources and Department of Geology, University of California, Davis, CA 95616, USA.

*To whom correspondence should be addressed. E-mail: furrer@ito.umnw.ethz.ch (G.F.); whcasey@ucdavis.edu (W.H.C.)

Table 1. Characterization of the selected field samples of representative aluminum oxyhydroxide flocs, collected from 1996 to 2001. Some samples were centrifuged immediately after collection and then dried under ambient conditions. Other samples (e.g., those from Spenceville) were analyzed both as a wet paste and as an air-dried gel. The aluminum concentrations were measured in the 0.45 μm–filtered water samples from the mixing zones. For the sample shown in Fig. 2A, middle, values are not available from direct in situ measurements in the mixing zone because the acid mine effluent (pH = 2.3; 1 mM < ΣAl < 15 mM) enters the pristine stream water [pH = 7.7; ΣAl < detection limit (d.l.)] from the hyporheic zone.

Sample spectrum	Geographic region	Geology	Vegetation	Type of pollution	Sampling date	pH in mixing zone	Aluminum concentration
Fig. 2A, top	East Thuringian, Slate Mountains, Germany	Carboniferous blue slate	Mixed forest	Acid mine drainage	22 May 1998	5.0 to 6.5	20 to 180 μM
Fig. 2A, middle	Spenceville, Yuba County, California	Metavolcanic rocks	Mixed forest	Acid mine drainage	4 Jan 2001	—	0 to 16 mM
Fig. 2A, bottom	Ore Mountains, Saxony, Germany	Mica slate, gneisses	Spruce	Acid rain	25 Mar 1999	5.0 to 5.5	18 to 60 μM